Additive Manufacturing 28 (2019) 14–22

Contents lists available at ScienceDirect

Additive Manufacturing

journal homepage: www.elsevier.com/locate/addma

Full Length Article

Cellulose nanocrystals support material for 3D printing complexly shaped structures via multi-materials-multi-methods printing

Vincent Chi-Fung Li[a,b], Xiao Kuang[c], Craig M. Hamel[a,c], Devin Roach[c], Yulin Deng[a,b,*], H. Jerry Qi[a,c,*]

[a] Renewable Bioproduct Institute, Georgia Institute of Technology, Atlanta, GA 30332, USA
[b] The School of Chemical & Biomolecular Engineering, Georgia Institute of Technology, Atlanta, GA 30332, USA
[c] The George W. Woodruff School of Mechanical Engineering, Georgia Institute of Technology, Atlanta, GA 30332, USA

ARTICLE INFO

Keywords:
Cellulose nanocrystals
Hybrid 3D printing
Direct-ink-write 3D printing
Inkjet 3D printing

ABSTRACT

To fabricate highly complex structures, sacrificial support material is usually needed. However, traditional petroleum-based support materials are un-sustainable, non-recyclable, and difficult to be completely removed from the target structure after 3D processing. Instead, cellulose nanocrystals (CNC) gel could serves as an interesting 3D printing support material due to its sustainability, renewability, and potential recyclability. Since CNCs are highly dispersible in water as nanoparticles and are also not UV sensitive, it has less absorption or bondability with other UV curable polymer matrices. This allows them to be completely washed out by water, which offers a green and efficient method to remove the CNC support material during post processing. In addition, with increasing needs for more intricate structures, combining different 3D printing strategies into a hybrid 3D printing platform can be highly beneficial. In this work, a multi-materials-multi-methods (M^4) printer with dual direct-ink-write (DIW) and DIW-inkjet printing capability was used to fabricate various complex structures while using CNC as support material. After 3D printing, water was used to remove the CNC support structure. Even in a highly confined environment, such as the inside of a balloon structure, CNC support material was still easily removed. The potential of using sustainable CNC support material and M^4 hybrid 3D printing strategies to fabricate different complex structures was demonstrated. Since CNC gel is derived from forestry products and is entirely water based, the 3D printing process was also made more environmentally friendly, sustainable, and potentially recyclable.

1. Introduction

3D printing technologies have seen significant development in the past decade, in part due to many different varieties of 3D printers becoming available [1–6]. According to ASTM classification standards, the seven main types of 3D printing techniques are material extrusion, material jetting, vat photo-polymerization, powder bed fusion, reactive binder jetting, directed energy deposition, and stacked sheet lamination [7]. Depending on the type of 3D printer used, materials with different properties are required for proper 3D processing. For example, direct ink write (DIW) 3D printing, a form of material extrusion, requires high viscosity ink with appreciable shear thinning behavior for material deposition and shape holding during 3D printing. In contrast, inkjet based 3D printing requires low viscosity ink with strict control on physical properties such as stable surface tension. As a result, different materials have their own unique processing requirement needs, while also providing different properties and functionalities to the final printed part.

The concept of hybrid 3D printing has also been steadily gaining popularity, as it combines multiple 3D printing techniques with different processing tools like robotic arm pick-and-place (P + P) or spray coating technologies into an integrated fabrication platform [8–12]. Hybrid 3D printing is also able to take advantage of the unique processing capability of each 3D printing technique to print different materials, and produce intricately shaped and multi-functional structures that are made of heterogeneous materials. For example, Valentine et al. utilized DIW 3D printing to print conductive and dielectric elastomer, and then used robotic arm P + P to insert electronic components within the target structure during 3D printing [13]. The resultant structures demonstrated potential application in wearable electronics, soft robotics, and biomedicial devices. Tong et. al. also utilized a DIW based extrusion technique and a robotic arm P + P system to fabricate nerve

* Corresponding authors at: Renewable Bioproduct Institute, Georgia Institute of Technology, Atlanta, GA 30332, USA.
E-mail addresses: yulin.deng@rbi.gatech.edu (Y. Deng), qih@me.gatech.edu (H.J. Qi).

https://doi.org/10.1016/j.addma.2019.04.013
Received 5 November 2018; Received in revised form 8 March 2019; Accepted 16 April 2019
Available online 17 April 2019
2214-8604/ © 2019 Elsevier B.V. All rights reserved.

cuffs with locking mechanisms that are suited for neural interfacing related applications [14]. Yoon et al. combined inkjet printing and spray coating techniques to fabricate 3D hydrogel structures suitable for potential tissue engineering applications [15]. Raza et al. was able to combine both DIW and inkjet 3D printing methods together in order to process a multi-materials 3D part that is composed of metal, rubber, and plastics, and demonstrated the highly extended manufacturing capability of hybrid 3D printing technology [16]. Other works have also demonstrated the possibility to utilize different hybrid 3D printing strategies, such as dual FDM 3D printing [17], multi-materials-multi-technology stereolithographic 3D printing [18], and stereolithographic-DIW 3D printing [19], to fabricate highly complex and functional structures that are composed of multiple materials. Overall, with increasing needs and demands for more complex and intricate 3D structures, it is conceivable that combining different 3D printing techniques into a single multi-materials-multi-methods (M^4) 3D printing platform can be highly beneficial.

During 3D printing, a sacrificial support material is usually a critical component for the successful fabrication of highly complex objects. This is because overhanging or bridge like features in 3D structures can only be fabricated when the depositing target material is laid on top of a sacrificial support structure. Otherwise, the depositing target materials would simply deform from the intended printing shape due to viscous thread instability or gravitational forces. Depending on the 3D printing methods and the complexity of structures, support materials can be more than 50% of the total materials used in a 3D printing job. Overall, many different support materials or support baths can be used in different 3D printing techniques [20–25]. For example, uncured powder particles remain on the build platform and serve as support material during selective laser sintering (SLS) 3D processing. During digital light processing (DLP) 3D printing, the photocurable polymer resin is sometimes cured to from small cylinders or pillars that serve as supporting structures. In inkjet printing, printhead jettable monomers and polymers have also been utilized as support material in various commercial 3D printers [26]. In regard to DIW 3D printing, both inert gel and hydrogel suspension bath have been used as support materials [22–25]. In fact, Hinton et al. developed a fugitive gelatin slurry for support bath, which can be released from the target structure by heating it to 37 °C in order to melt the gelatin [25]. Nevertheless, traditional support materials are usually un-sustainable and non-recyclable because they are typically polymerized or solidified along with the target structure. During post processing, this can also make it difficult to remove the support material. In some cases, caustic solvent, such as sodium hydroxide or alkaline bath, is needed in order to efficiently remove the support material [27]. This can generate excess waste due to a large quantity of solvents has to be used, which creates the issue of environmental pollution and is non-sustainable. Therefore, there is a strong need to develop environmentally friendly and sustainable inks for support materials. Cellulosic nanomaterials, such as cellulose nanocrystals (CNC) and cellulose nanofibers (CNF), can be derived from trees, plants, and even agricultural residues [28–30]. These cellulosic resources are abundantly available, recyclable, and sustainable, which can be utilized to make 3D printing more sustainable and environmentally friendly [31–34].

Previously, we have demonstrated the ability of using DIW 3D printing to print CNC and CNF gels into highly customizable 3D structures with controllable properties, quality, and resolution [35,36]. These DIW 3D printable gels are entirely cellulosic in nature and water based. For example, CNCs were mixed directly with water in order to produce a CNC gel that can be easily processed by DIW 3D printing. Compared with traditional petroleum based polymeric support materials used in 3D printing, CNCs suspended in water are in nanoparticles form and are also non-UV light sensitive. As a result, CNC gel is less absorbable onto other polymer matrices that are cured by UV light, which allows them to be completely washed away with water during post processing of 3D printing. In this work, we explore the feasibility of using CNC gel as supporting material in both dual DIW and DIW-inkjet hybrid 3D printing in order to fabricate various complexly shaped structures. After 3D printing, the CNC gel was removed quickly and efficiently using water in order to produce the final target structure. The potential of using CNC gel as support material and M^4 hybrid 3D printing to fabricate highly complex structures was demonstrated. Since CNC gel is derived from forestry products and is entirely water based, using CNC gel as support materials can make the 3D printing process more environmentally friendly, sustainable, and potentially recyclable.

2. Experimental

Freeze dried CNCs were purchased from University of Maine Process Development Center (Orono, ME, USA), and used as received. Butyl acrylate, polycaprolactone (Mn of 70,000–90,000), fumed silica powder (0.2 to 0.3 μm particles), and phenylbis(2,4,6-trimethylbenzoyl) phosphine oxide (Irgacure 819) were purchased from Sigma-Aldrich (St. Louis, MO, USA) and used as received. An UV curable aliphatic urethane diacrylate (EBECRYL 8413) based oligomer was kindly donated by Allnex Inc. (Alpharetta, GA, USA) and used as received. UV curable inkjet ink (ETIJET ULX5832 CYAN) was purchased from SunJet DIC Inkjet Solutions (Parsippany, NJ, USA) and used as received.

CNC aqueous gel (20 wt %) was prepared as according to our previous work [35]. Briefly, CNC gel was prepared by mixing an appropriate amount of freeze dried CNC and water together through probe homogenization at 10,000 rpm. Also adopted from our previous work with minor modifications [37], an elastomeric resin that is UV curable was prepared by first mixing polycaprolactone with butyl acrylate, and then stirred with a magnetic stir bar at 70 °C until the polycaprolactone was fully dissolved. While keeping the resin around 70 °C to improve mixing, a 1:1 mass ratio of EBECRYL 8413 was added to the dissolved polycaprolactone-butyl acrylate solution, and then was mixed by hand until a homogenous resin is obtained. Irgacure 819 and fumed silica were subsequently added and mixed by hand until a homogenous elastomeric resin was obtained (Formulation: 46.5 wt % butyl acrylate, 0.7 wt % polycaprolactone, 46.5 wt % EBECRYL 8413, 1.5 wt % Irgacure 819, and 4.8 wt % fumed silica). The butyl acrylate serves as the main monomeric component for polymerization, EBECRYL 8413 is a high molecular weight cross-linker that increases the stretchability of the polymer, and polycaprolactone is a high molecular thermoplastic that allows the viscosity and T_m of the resin to be adjusted. Irgacure 819 serves as the photo-initiator, and fumed silica is added as a rheology modifier that imparts shear thinning effect to the elastomeric resin. Overall, the final elastomeric resin's container was wrapped in aluminum foil, and then stored at room temperature until further use. Before DIW 3D printing, the CNC gel and the elastomeric resin were placed in separate syringes. To ensure all air bubbles were removed from the syringes, centrifugation processing was performed at 5000 rpm for 10 min.

The multi-materials-multi-methods (M^4) printer is comprised of a printing stage that is controlled by the Aerotech Inc. motion system (Pittsburgh, PA, USA), where the stage can travel between different printing modules. In this work, a DIW system with dual material deposition capability, and a piezoelectrically driven drop-on-demand inkjet print head (Xaar, Cambridge, United Kingdom) with UV lamp attachment (FE300UV LED lamps, Phoseon Technology, Hillsboro, OR, USA) were used. The M^4 printer was also pre-configured with positional offset optimizations for each module, so that all the printing modules are aligned and can properly interact with one another.

The DIW system utilizes a pneumatic dispenser (Ultimus V, Nordson EFD, East Providence, RI, USA) to controllably extrude printing materials from syringes using specified compressed air pressures. The movement of the syringe was programed to follow the g-code generated by the in-house developed software, which uses STL file obtained from SolidWorks as the input. By controlling the pneumatic deposition and the syringe movement, one layer of the 3D structure can be formed line-

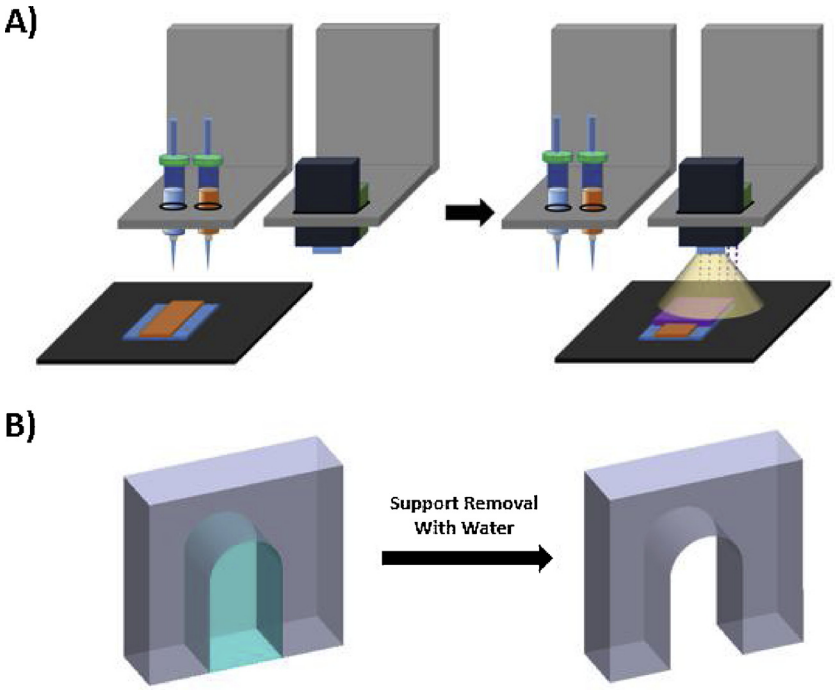

Fig. 1. (A) Schematic illustration of the dual DIW and DIW-inkjet 3D printing processes. (B) Schematic illustration of using water to remove the CNC support material in order to produce the final target structure.

by-line. Ultimately, the entire 3D structure can be fabricated in a layer-by-layer manner. In order to print two materials using the same DIW system, a switching unit was developed to direct compressed air between two separate syringes. The generated g-code can also instruct the switching unit to direct the compressed air to the syringe holding the elastomeric resin when printing the target structure, or re-direct the air to the syringe holding the CNC gel when printing the support structure. A printing pause was inserted in between each switching action, which allowed the deposition pressure to be adjusted depending on which material was to be deposited next. In this manner, a single layer comprised of both the elastomeric resin and the CNC gel can be printed. After each layer of the structure was deposited, the built stage was moved under the UV lamp for polymerization. Through trial and error, the optimal movement speed of the elastomeric syringe was found to be 10 mm/s, whereas the movement speed of the CNC syringe was found to be 40 mm/s. Meanwhile, the extrusion pressure for the elastomeric resin and the CNC gel were respectively set at around 10 psi and 8.5 psi in order to produce extruded filaments with width that closely matched with the inner diameter of the nozzle tip. The inner diameter of the tapered type nozzle attached to each syringe was 400 μm.

The inkjet system utilizes an inkjet supply system (Hydra, Xaar, Cambridge, United Kingdom) to achieve proper meniscus pressure and temperature control for consistent inkjet resin deposition from the Xaar print head. The SolidWorks design of the inkjet structure was first formatted as a STL file, and then processed with the in-house developed software into grayscale images. These images were loaded to the Xaar print head and controlled the shape of each deposited inkjet layer. After each inkjet layer was deposited, it immediately passed over the UV lamp in order to polymerize the layer. The corresponding support structure was processed similarly as before using the in-house developed software, and then was integrated together with the inkjet processing instructions to produce the final g-code script for 3D object fabrication via DIW-inkjet.

While under a room temperature of about 22 °C, the viscosity of the elastomeric resin, the CNC gel, and the inkjet ink were analyzed by the DV2TLV and DV3THV cone and plate viscometers (Brookfield Engineering Labs Inc., Middleboro, MA, USA). Cone spindles of CPA-40Z, CPA-41Z, and CPA-52Z were used. Cone plates of CPA-44YZ and CPA-44PSYZ were also used during the viscosity characterization. Viscosity was measured as a function of shear rate, where the shear rate ranged between 0.2 s^{-1} and 500 s^{-1}. A minimum of 10 measurements were collected for each sample at each corresponding shear rate, and averaged values were reported. The gap separation between the spindle and the plate was set at 0.013 mm. To minimize potential wall slip effects, about 3 g of resin or gel was distributed across the entire plate surface before each characterization was performed.

Elastomeric and inkjet layers that were sandwiched between two CNC gel layers were fabricated through dual DIW or DIW-inkjet 3D printing. After the CNC gel support was removed with water, both the topside and the underside of the dried elastomeric and inkjet layers were analyzed by ATR-FTIR (Nicolet iS50, ThermoFisher Scientific, Waltham, MA, USA) spectrometer under ambient conditions from an average of 32 scans with a scan resolution of 1 cm^{-1} in the range of 600 cm^{-1} to 4000 cm^{-1}. After the topside of the layer was characterized, FTIR analysis was preformed again after the layer was flipped over to the underside. Spectra for pure CNCs were analyzed by placing freeze dried CNC powder onto the sampling lens.

The washed and dried elastomeric and inkjet layers were first attached to the SEM sample holders with conductive double-sided tape, and then sputter coated (Q-150 T ES Sputter, Quorum Technologies, Laughton, East Sussex, London) with gold for 30 s at 20 mA current. Then, SEM imaging (LEO 1530, Zeiss, Jena, Germany) was performed at 20 kV accelerating voltage.

3. Results and discussion

3.1. Dual DIW and DIW-inkjet hybrid 3D printing

The dual DIW and the DIW-inkjet 3D printing process were used to construct various complexly shaped structures. During dual DIW 3D printing, both the elastomeric resin and the CNC gel were deposited onto the printing stage. Then, the printing stage moved over to the UV lamp unit, where the elastomeric resin was polymerized. Since the CNC gel is not photocurable, the gel remained as a gel structure that served

as the support structure for the next deposition layer. Similarly, the DIW-inkjet printing process worked by depositing the CNC gel with DIW, while the inkjet ink was deposited by the Xaar print head and then polymerized by UV light irradiation. As a result, a 3D structure consisting of either elastomeric resin and CNC gel, or inkjet ink and CNC gel was printed through a layer-by-layer manner. The multi-materials-multi-methods (M^4) printer containing both the dual DIW 3D printing module and the DIW-inkjet 3D printing module is illustrated (Fig. 1A and Supplementary Figure S1), and their respective printing processes are also provided (Supplementary Video SV1 and SV2). After 3D printing, the overall concept is to use water to efficiently remove the sustainable CNC gel support material, and then produce the final target structure (Fig. 1B).

3.2. Rheology of elastomeric resin, DIW gel support, and inkjet printing ink

During dual DIW and DIW-inkjet 3D printing, the rheology of the resin, gel, and ink is an important criterion to consider. The DIW processable material must have high viscosity such that the printed shape can be maintained, and it must also be shear thinning so that extrusion through the nozzle is possible during deposition. The rheological behaviors of both the elastomeric resin and the CNC gel were characterized, and it was clear that both the resin and the gel displayed appreciable shear thinning effect (Fig. 2A). In fact, their viscosities decreased by over three orders of magnitude in the shear rate range between 0.2 and 500 s^{-1}. This supports that both the elastomeric resin and the CNC gel can flow efficiently during DIW 3D printing because high shear is applied across the nozzle as the inks are deposited. Once they were deposited, their high viscosities ensured that the printed shapes were maintained without any structural sagging. In addition, previous literatures have also demonstrated that the yield stress of 20 wt % CNC gel can be as high as 350 Pa [38,39], which makes CNC gel a good candidate as support material. On the other hand, the inkjet ink displaced the required Newtonian behavior, where the viscosity was kept relatively low at around 42 ± 1 cP regardless of shear rate.

3.3. FTIR characterization of CNC gel support removal

Both the dual DIW and DIW-inkjet 3D printing process began by first designing the target structure and the corresponding support structure using SolidWorks. As an initial demonstration, a structure with an elastomeric layer (colored orange) sandwiched between two CNC gel layers (colored light blue) was fabricated through dual DIW 3D printing. The SolidWorks model, the as-printed structure, and the final obtained structure after CNC support removal with water are correspondingly illustrated from left to right (Fig. 2B). Similarly, a structure with an inkjet layer (colored purple) that was sandwiched between two CNC gel layers was also fabricated through DIW-inkjet 3D printing. The resultant as-printed structure, and the final obtained structure after water washing are also illustrated (Fig. 2C).

To study the effectiveness of using water to remove CNC gel from both the elastomeric and the inkjet surfaces, the previously fabricated sandwiched elastomeric and inkjet layers were analyzed using FTIR methods (Fig. 3A and B). For comparative purposes, an elastomeric layer and an inkjet layer without any CNC gel layer sandwiching were also fabricated with the M^4 printer. The FTIR spectra for pure CNCs were first obtained in order to evaluate if there are any CNCs debris left on the washed elastomeric or inkjet layers. CNCs exhibited a FTIR spectrum with peaks at wavenumbers of 895 cm^{-1}, 1030 cm^{-1}, and 1050 cm^{-1}, which are cellulose's characteristic peaks for C—O—C deformations of the β 1–4 glycosidic bond, C—O—H stretching in the pyranose rings, and C—O—C vibrations in the cellulose pyranose rings. Other peaks between 1110 cm^{-1} and 1430 cm^{-1} are also characteristics peaks for cellulose's C–O, C—C, C–H, and C—O—H related vibrations. Most importantly, the major peaks at 2900 cm^{-1} and 3330 cm^{-1} were also present, which are attributed to C–H stretching and O—H stretching in absorbed water and in cellulose [40–45]. Comparing FTIR spectra from CNCs and that from a DIW 3D printed elastomeric layer without any CNC sandwiching, the most drastic differences were the peak emergence at 1730 cm^{-1} and the peak disappearance at 3330 cm^{-1} (Fig. 3A). The peak at 1730 cm^{-1} can be attributed to the C═O ester vibrations in acrylate related functional groups [46]. At the same time, the absence of cellulosic material also led to the major O—H vibrational peak (3330 cm^{-1}) related to absorbed water on cellulosic surfaces and hydroxyl functional groups within cellulosic structures to significantly reduce. The same phenomena were observed in the spectra for both the topside and the underside of the washed elastomeric layers that were sandwiched between CNC gel layers, which suggested that water was also able to effectively remove CNC from the elastomeric surfaces. In fact, spectra for elastomeric layer without and with CNC sandwiching were practically identical. As a result, FTIR analysis supported that water can effective remove the CNC gel from both the topside and the underside of elastomeric material. This could also be attributed to the fact that the elastomeric material is hydrophobic in nature, which also helped prevent any potential diffusion between the CNC gel and the elastomeric material. Similar observations were also seen for the FTIR analysis for the inkjet layers, where the significantly reduced peak intensity at 3330 cm^{-1} suggested that practically all CNCs were removed on both the topside and the underside of the inkjet layer after water washing (Fig. 3B). While the inkjet material is hydrophilic, there also appeared to be negligible diffusion between the CNC gel and the inkjet material due to the short processing time between when the inkjet material was deposited from the print head and when the inkjet material was cured by the UV lamp. This was further supported as the resultant CNC suspension after water washing remained cloudy white that is indicative of a pure CNC suspension, while also having no discoloration from the highly cyan colored inkjet material.

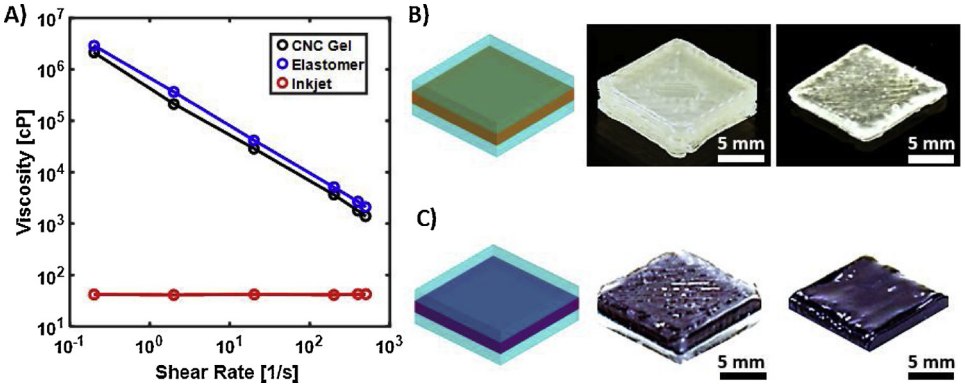

Fig. 2. (A) The viscosity versus shear rate curves at room temperature for the elastomeric resin, CNC gel, and inkjet ink are illustrated. (B) Left: The SolidWorks model of an elastomeric layer sandwiched between two CNC layers is presented. Middle: The as-printed structure after dual DIW 3D processing. Right: The final obtained target structure after washing away the CNC support material with water. (C) Similarly, the corresponding model and structures from DIW-inkjet 3D processing of an inkjet layer sandwiched between two CNC layers are presented.

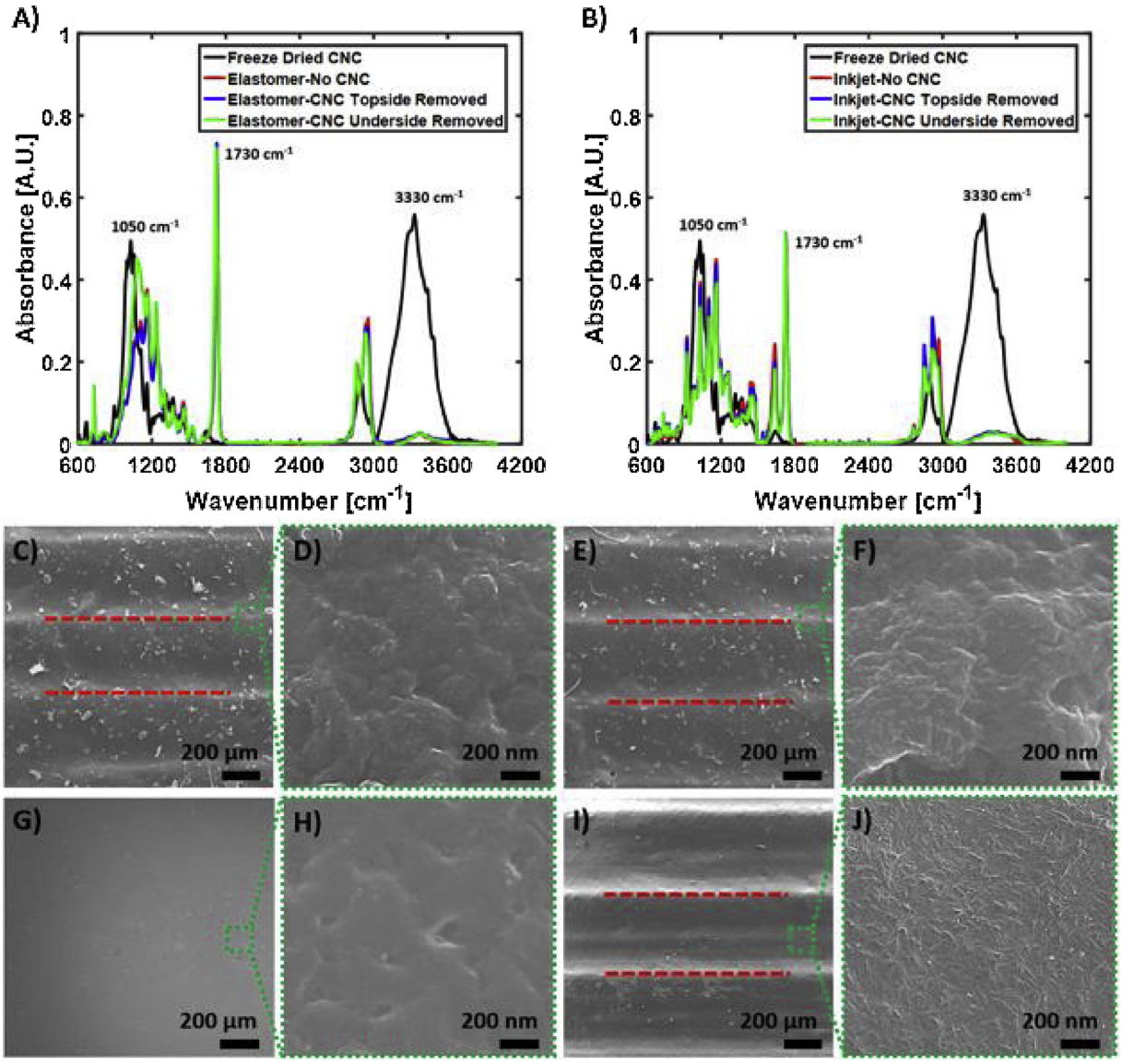

Fig. 3. (A) The FTIR spectra for the freeze dried CNCs (black), the dual DIW 3D printed elastomeric layer without any CNC deposition (red), the topside of the dual DIW 3D printed elastomeric layer that was sandwiched between two CNC gel layers (blue), and the corresponding underside of the elastomeric layer (green) are illustrated. (B) The corresponding FTIR spectra for the analysis of the inkjet layer processed with DIW-inkjet 3D printing. (C) Low magnification SEM images of the dual DIW 3D printed elastomeric layer's topside. The red dash lines in the low magnification images showcase the width of the filament like features. (D) The corresponding SEM image taken at high magnification, where the filaments' interfacial bonding is illustrated. (E) Low magnification SEM images of the dual DIW 3D printed elastomeric layer's underside. (F) The corresponding SEM image taken at high magnification, where the filaments' interfacial bonding is again illustrated. (G) Low magnification SEM images of the DIW-inkjet 3D printed inkjet layer's topside. (H) The corresponding SEM image taken at high magnification. (I) Low magnification SEM images of the DIW-inkjet 3D printed inkjet layer's underside. (J) The corresponding SEM image taken at high magnification.

3.4. SEM characterization of xyz-directional surface morphology

The xy-directional surface morphology of the elastomeric and inkjet layers was also studied through SEM characterization. Both the topside and the underside of the elastomeric and inkjet layers that were sandwiched between CNC gel layers were analyzed (Fig. 3C to 3 J). The topside of the elastomeric layer showed that the surface has filament like features (Fig. 3C). In fact, ImageJ analysis confirmed that the filament like features (red dash lines) have a width of about 400 µm, which matched closely with the inner diameter of the nozzle tip that was used during DIW processing. The DIW printed elastomer filaments are also well bonded together (Fig. 3D), as higher magnification SEM images showed that the elastomeric filaments are well attached together without significant separations or defects. Similarly, lower magnification image of the elastomeric layer's underside also illustrated filament like features (Fig. 3E), and the corresponding higher magnification image showcased that the filaments are also well attached to one another (Fig. 3F). On the other hand, the topside of the inkjet layer displayed morphology of an extremely smooth surface at both low and high magnification (Fig. 3G and 3 H). Meanwhile, the underside of the inkjet layer displayed filament like features (Fig. 3I). ImageJ analysis again confirmed that the width of each filament features is approximately 400 µm (red dash lines). The difference between the inkjet's topside and underside surfaces could be explained by the low viscosity of the inkjet ink and the DIW-inkjet processing steps. As the first CNC gel layer in the sandwiched structured was formed, the layer likely also has filament like features because the CNC gel has similar rheological properties as the elastomeric resin. When the inkjet layer was then deposited, the low viscosity inkjet ink was likely able to flow into the interfacial filament spaces left behind by the underlying CNC gel

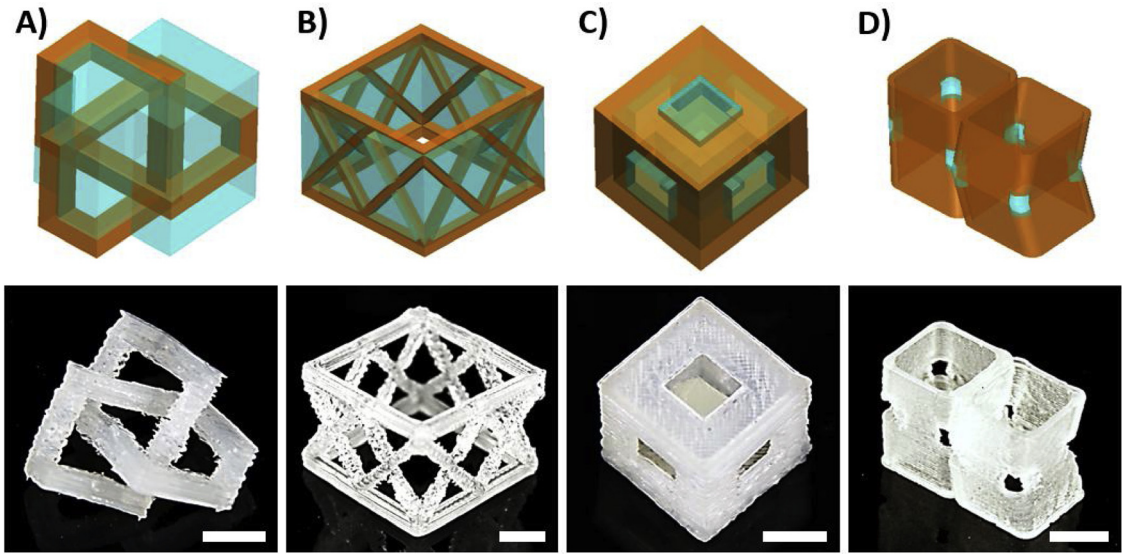

Fig. 4. The SolidWorks models (top) and the resultant dual DIW 3D printed structures with support removed (bottom) are illustrated. Various structures include (A) cubic trefoil knot, (B) box with cross frame as boundary, (C) box frame containing a cube within its center, and (D) a zippered origami tube. Displayed scale bars are 1 cm.

filaments. Afterwards, the layer was then polymerized with UV light to produce a negative image of the underlying filament like CNC gel layer. As more inkjet layers were deposited, the surface morphology became highly smooth because any further defects and features left on the surface were gradually filled by the low viscosity inkjet fluid and then UV polymerized. When the second CNC gel layer in the sandwiched structured was formed, the underlying inkjet layer was already UV polymerized into a solid layer, so subsequent CNC gel filament deposition no longer had any effect on the topside's smooth surface morphology. Interestingly, the higher magnification SEM image for the inkjet's underside displayed a surface morphology that resembled tightly packed CNCs (Fig. 3J). Typically, a low SEM accelerating voltage of no greater than 10 kV is usually used when preforming SEM imaging of cellulosic or biological materials in order to avoid burning effects [47]. Since a SEM accelerating voltage of 20 kV was used and there was no burning effect observed during SEM imaging, it supported that the observed tightly packed CNCs surface morphology did not result from CNCs that were left on the underside surface of inkjet layer. Instead, it was more likely that the inkjet ink formed a negative image of the CNCs on the underlying CNC gel layer, as the low viscosity inkjet ink was able to adopt to even the nanoscale morphological features of CNCs before it was polymerized by the UV lamp. This was further supported by the FTIR analysis, where the CNC dominant peak at 3330 cm^{-1} was not prominent for the inkjet layer's underside. As a result, the low viscosity inkjet ink not only created a negative image of the underlying features at the macroscopic level (the filament like features), but also surface morphologies at the nanoscopic level (tightly packed CNCs like features).

Furthermore, the z-directional morphological features of the elastomeric and inkjet structures were also characterized by SEM (Supplementary Figure S2), where two different z-directional surfaces were analyzed. The first was the free side surface, which represented the z-directional surface that was fabricated without any CNC support next to it. The second was the interface side, which represented the z-directional surface that was fabricated with the CNC support structure next to it. It was again observed that the elastomeric z-directional surface was composed of filaments of about 400 μm thickness on both the free side and the interface side, where each filament appeared to be well bonded with one another. During inkjet printing, the resolution of each deposited inkjet layer was estimated to be 30.8 μm per pass over the print head. The inkjet layer thicknesses as a function of number of passes over the print head were analyzed using a Thickness Tester (Supplementary Figure S3). On the other hand, the resolution of DIW printing is limited by the inner diameter of the nozzle tip. In this case, tapered nozzles with an inner diameter of 400 μm were used to deposit the CNC gel support material. During layer-by-layer formation in the 3D printing process, it then became necessary to match the layer thickness of both the inkjet and the CNC material within each sliced layer of the 3D structure. Since the Thickness Tester evaluated inkjet thickness for 13 passes was approximated to be about 405.9 ± 0.9 μm, a total of 13 inkjet deposition passes was performed to match with the layer resolution of each CNC gel layer deposition. Through repeating cycles of 13 inkjet depositions to one CNC gel deposition to form each layer, structures made of polymerized inkjet material and CNC support material can be fabricated. During SEM analysis, the free side of the inkjet structure's z-directional surface did not exhibit filament like features, but instead displayed a relatively smooth surface with beads like surface roughness. The beads like features could be attributed to the low viscosity inkjet ink still had the ability to flow when the stage was moving to the UV lamp, so the ink slightly flowed pass the layer's outer boundary in the xy-direction and cascaded down the z-direction before it was polymerized. When the interface side of the inkjet structure was analyzed, filament like features that resulted from the negative image of the CNC gel layers was again observed. The filament features on the inkjet structure's z-directional interfacial surface also had a thickness of approximately 400 μm, which again supported that 13 inkjet passes were required to match the filament thickness of each CNC gel layer. Upon higher magnification, a negative image of the CNCs resulting from the adjacent CNC gel layer was again observed. Overall, it was confirmed that water can effectively remove the CNC gel from both the elastomeric surfaces and the inkjet surfaces. Furthermore, unique surface morphologies can be left behind depending on the 3D printing strategy employed, and on whether the CNC gel was deposited next to the structure.

3.5. Structures printed with dual DIW hybrid 3D printing

Utilizing CNC gel as support materials, various demonstrational but complex structures such as a cubic trefoil knot, a box with cross frame as boundary, a box frame containing a cube within its center, and a zippered origami tube were 3D printed through the dual DIW printing approach (Fig. 4). A cubic trefoil knot with beams that looped within

itself was successfully printed, and this print was only made possible with support material because separation between beam components was necessary during DIW 3D processing (Fig. 4A). In this case, the CNC gel served as a sustainable, renewable, and green support material, which offered significant advantage compared to traditional petroleum-based support materials. Support removal is also made significantly easier, as the CNC gel was quickly and efficiently removed using water because CNC nanoparticles have less bonding tendency with other UV curable polymeric surfaces. Since the CNC gel was originally made in water, the resultant CNC suspension generated during support removal can even be potentially re-processed back into a gel with the appropriate CNC concentration through freeze drying and re-dispersion so that it is suitable for DIW 3D printing again. In another instance, a box with cross frame as boundary was also successfully fabricated using CNC support material and dual DIW 3D printing (Fig. 4B). Typically, DIW 3D printing of pillars in the z-direction without any support material is difficult because of pillars' location displacement with gravitational effect or other processing related factors. While using CNC gel as support, this phenomenon was significantly reduced because the CNC gel ended up limiting the movement of the pillars during DIW printing. This allowed each layer of the pillars to be accurately deposited on top of each other, which allowed a highly difficult structure such as a box with cross frame as boundary to be successfully fabricated. In another demonstration, it was also demonstrated that CNC gel can be printed between two different target structures in order to produce a box frame containing a cube within its center (Fig. 4C). Once the CNC gel was removed, a contained cube can be rattled inside the box frame. To further demonstrate the ability to use CNC gel as support material to fabricate highly complex objects, a bi-directionally foldable zippered origami tube structure was fabricated (Fig. 4D). Typically, two mirrored miura-ori units are first stacked together in order to from an origami unit. Then, two origami units are attached together on their side via a zig-zag manner in order to from a zippered origami tube structure [48,49]. Here, the fabrication of the zippered origami tube structure was made significantly easier because the structure was directly 3D printed in a one-step processing approach instead of the traditional multi-steps fabrication and assembly approach. During 3D fabrication of origami tubes, it is also necessary to introduce holes near the hinge regions and at the apex of fold lines. Otherwise, the origami tube structure can be easily damaged or can be difficult to be folded during its 2D and 3D shape re-configuration [50]. In this case, CNC gels support material was utilized in the fabrication of the origami tube's hinge and apex regions. After support removal with water, the origami tube was able to repeatedly re-configure from a 3D shape into a 2D shape in the y- and z- axes, while the structure remained relatively stiff in the x-axis (Supplementary Figure S4). This type of origami tube structure can have potential applications in solar arrays, robotics, deployable canopies, outer space architectures, and many others [50–52].

In addition, 3D printing a hollow sphere like structure in a layer-by-layer manner is usually difficult because the radius of each ring in the layer is constantly changing during the hollow sphere's fabrication. For example, as the radius of the ring increases, it becomes increasing difficult to use DIW to properly deposit the ink filament into the desired ring shape because of viscous thread instability effect. As a result, 3D printing technique like digital light processing is usually used to process hollow structures, where the need for support material is not necessary [53]. Nevertheless, it is still be possible to use support material during DIW based 3D printing in order to help with the fabrication of hollow structures. In this case, CNC gel can be used as the support material within a hollow balloon structure, which can help minimize viscous thread instability effect because the outer boundary of the deposited CNC layer can serve as an outline for the elastomeric filament to follow. In effect, the elastomeric ring layer will be contained between air and the CNC gel instead of between air on both sides. In this regard, a balloon structure and its corresponding support structure were first fabricated with SolidWorks (Fig. 5A). Afterwards, a balloon structure was successfully fabricated while using CNC as support material (Fig. 5B). Furthermore, it was demonstrated that even in a highly confined environment, such as the inside of a balloon, water was still able to easily remove the CNC support material (Supplementary Video SV3). In fact, the balloon was cut in half, and qualitative visual inspection supported that the all of the CNC gel was successfully removed from the inside of the balloon (Fig. 5C). Additionally, the elastomeric rings were not only well bonded with one another, but our previous study had also shown that the polymerized elastomer has a strain before break of up to 600% [37]. Since the polymerized elastomer is highly stretchable and the layer interfaces are well bonded together, it is possible to use air to reversibly inflate the 3D printed balloon. The 3D printed balloon was also able to expand to more than eight times its original volume without having air leakage or structural damage (Fig. 5D and Supplementary Video SV4). Overall, it was demonstrated that CNC gel can be used as support material in many ways in order to print different variety of highly complex structures through the dual DIW 3D printing approach, and then water can be used to easily remove the support material during post processing. Nevertheless, there are still some limitations in using CNC gel as support material. For example, the CNC gel support removal process requires the main printing material to be curable with UV light or other similar mechanisms, such that it becomes water insoluble. In addition, other curing mechanisms that utilize heating can also be challenging due to potential water evaporation from the CNC gel. Furthermore, 3D printing CNC gel structures with extremely high resolution can also be time extensive due to the line-by-line printing nature of DIW processing. As a result, other more efficient printing techniques that are suitable for depositing CNC gel at high resolution can be a focus of future investigations.

3.6. Structures printed with DIW-inkjet hybrid 3D printing

CNC gel can serve as support material in not only DIW 3D printing, but also in other 3D printing techniques such as inkjet printing. Utilizing the DIW-inkjet printing approach while using CNC gel as support, a box with square and diamond opening on each side, a spiral, and a bridge were successfully fabricated (Fig. 6). During the 3D printing process, the inkjet ink was deposited onto the CNC support and then was immediately polymerized by UV light irradiation. Similar to the dual DIW printing process, the inkjet material is UV sensitive while the CNC gel is not. As a result, water can again be used to quickly remove the support material once the printing is completed. As a simple demonstration, a box with square and diamond opening on each side was first printed (Fig. 6A). In another instance, a spiral structure was also successfully printed (Fig. 6B). Furthermore, a bridge structure was also targeted for DIW-inkjet processing. In this case, CNC support was not only needed in the bridge's underside, but support was also needed on the topside during the fabrication of the bridge's suspensions and railings. After DIW-inkjet printing and the subsequent CNC support removal, an intricately shaped bridge was successfully fabricated (Fig. 6C). With the high-resolution print that is achievable through inkjet printing, other even more advance and complex structures can also be targeted in future investigations. Overall, it was demonstrated that CNC gel can also be used as support material in multiple different ways to form complex features within structures during DIW-inkjet 3D printing.

4. Conclusions

In conclusion, CNC gel was used as a sustainable support material during the fabrication of complex structures with a multi-materials-multi-methods (M^4) printer that has dual DIW and DIW-inkjet 3D printing capability. While traditional petroleum-based support materials are un-sustainable, non-recyclable, and are difficult to remove, CNC gel support material is sustainable, potentially recyclable, and can be easily removed using water. Both FTIR and SEM characterization

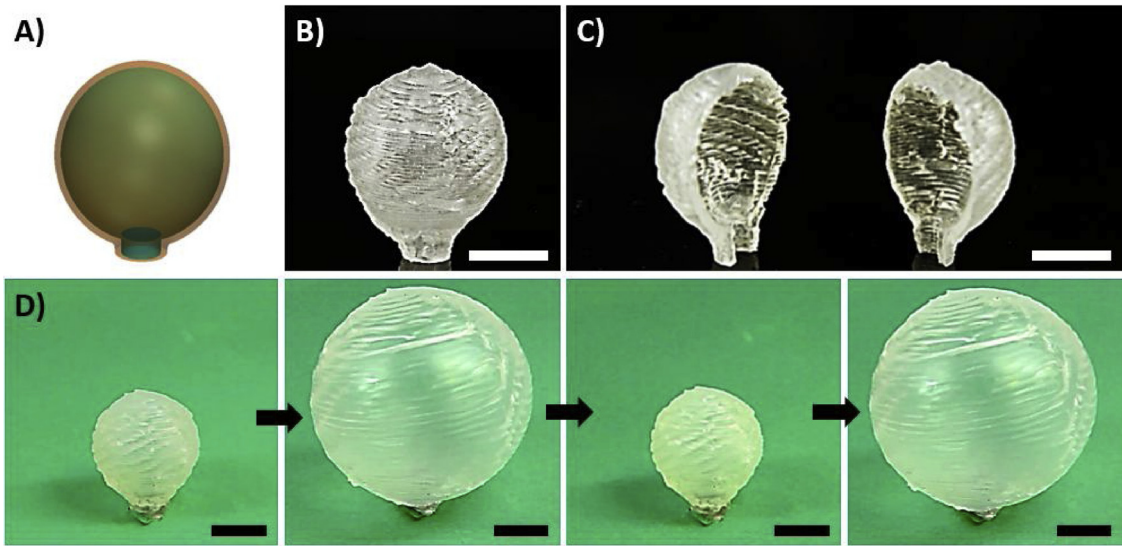

Fig. 5. Using the dual DIW 3D printing approach, a balloon structure was fabricated while CNC gel served as the support material. (A) The SolidWorks model of the balloon structure. (B) After CNC support removal with water, the final balloon structure is illustrated. (C) The resultant balloon is cut in half to showcase the successful removal of the CNC support material even in a highly confined environment. (D) Another balloon was fabricated, and the balloon's reversible inflation process using air is illustrated from left to right. Displayed scale bars are 1 cm.

illustrated that CNC gel was effectively removed from both the elastomeric surfaces and the inkjet surfaces during post processing with water washing. Furthermore, unique surface morphologies were left behind depending on which side of the structure the CNC gel was deposited and on which hybrid 3D printing method was used. Utilizing dual DIW 3D printing strategies, various complexly shaped structures were successfully fabricated while using CNC as support material. Even in a highly confined environment, such as the inside of a balloon, water was still able to easily remove the CNC support material during post processing. The interlayer adhesion of the elastomeric filaments was also demonstrated by the balloon's reversible inflation process. Not only was air not able to leak from the balloon during inflation, but the balloon was able to expand to at least eight times its original volume. CNC gel was also able to serve as support material during DIW-inkjet 3D printing, and various complexly shaped structures with intricate features were also successfully fabricated. Overall, these complex structures fabricated by CNC gel support material and the M^4 printer demonstrated potential for prototyping or other more advance applications.

Acknowledgements

The support of an Air Force Office of Scientific Research (AFOSR) grant (FA9550-16-1-0169; Dr. B.-L. "Les" Lee, Program Manager) and the National Science Foundation (NSF) award (CMMI-1462895) are gratefully acknowledged. Gift funds from HP, Inc and Northrop Grumman are also greatly appreciated. This work was performed in

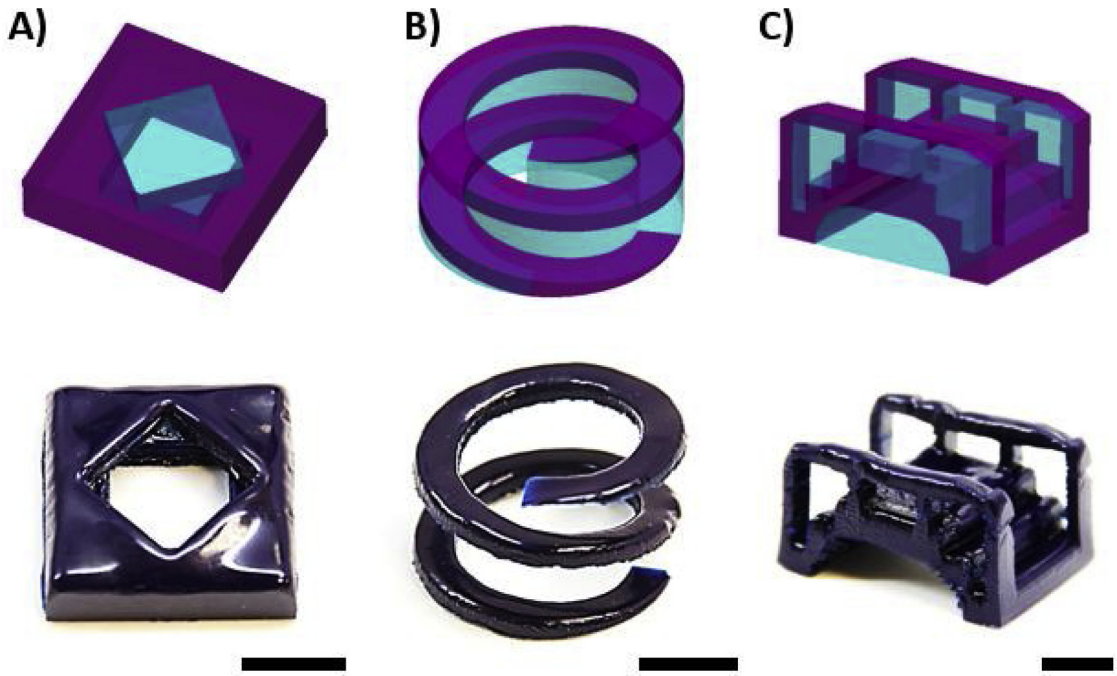

Fig. 6. The SolidWorks models (top) and the resultant DIW-inkjet 3D printed structures with support removed (bottom) are illustrated. Various structures include (A) a box with square and diamond opening on each side, (B) a spiral, and (C) a bridge. Displayed scale bars are 1 cm.

part at the Georgia Tech Institute for Electronics and Nanotechnology, a member of the National Nanotechnology Coordinated Infrastructure, which is supported by the National Science Foundation (Grant ECCs-1542174). The authors of this paper would like to thank the Renewable Bioproducts Institute at Georgia Tech for providing the PSE fellowship financial support. The authors also thank Professor S. Holger Behrens for the usage of the high viscosity cone and plate viscometer. The authors also thank Allnex Inc. (Alpharetta, GA, USA) for their kind donation of UV curable aliphatic urethane diacrylate (EBECRYL 8413) based oligomer.

Appendix A. Supplementary data

Supplementary material related to this article can be found, in the online version, at doi:https://doi.org/10.1016/j.addma.2019.04.013.

References

[1] J.K. Placone, A.J. Engler, Recent advances in extrusion-based 3D printing for biomedical applications, Adv. Healthc. Mater. 7 (8) (2018) e1701161.
[2] M. Layani, X. Wang, S. Magdassi, Novel materials for 3D printing by photopolymerization, Adv. Mater. 30 (41) (2018) e1706344.
[3] M. Nadgorny, A. Ameli, Functional polymers and nanocomposites for 3D printing of smart structures and devices, ACS Appl. Mater. Interfaces 10 (21) (2018) 17489–17507.
[4] Q. Wang, J. Sun, Q. Yao, C. Ji, J. Liu, Q. Zhu, 3D printing with cellulose materials, Cellulose 25 (8) (2018) 4275–4301.
[5] Z. Liu, M. Zhang, B. Bhandari, Y. Wang, 3D printing: printing precision and application in food sector, Trends Food Sci. Technol. 69 (2017) 83–94.
[6] S.C. Ligon, R. Liska, J. Stampfl, M. Gurr, R. Mulhaupt, Polymers for 3D printing and customized additive manufacturing, Chem. Rev. 117 (15) (2017) 10212–10290.
[7] ASTM, ASTM 52900-2015-E-Standard Terminology for Additive Manufacturing Technologies-General Principles Terminology, ASTM, ISO/ASTM International, 2016 p. 9.
[8] E. MacDonald, R. Wicker, Multiprocess 3D printing for increasing component functionality, Science 353 (6307) (2016).
[9] E. Macdonald, R. Salas, D. Espalin, M. Perez, E. Aguilera, D. Muse, R.B. Wicker, 3D printing for the rapid prototyping of structural electronics, IEEE Access 2 (2014) 234–242.
[10] A. Kataria, D.W. Rosen, Building around inserts: methods for fabricating complex devices in stereolithography, Rapid Prototyping J. 7 (5) (2001) 253–262.
[11] H.-S. Yoon, K.-H. Jang, E. Kim, H.-T. Lee, S.-H. Ahn, Hybrid 3D printing by bridging micro/nano processes, J. Micromech. Microeng. 27 (6) (2017) 065006.
[12] L. Wang, J. Liu, Compatible hybrid 3D printing of metal and nonmetal inks for direct manufacture of end functional devices, Sci. China Technol. Sci. 57 (11) (2014) 2089–2095.
[13] A.D. Valentine, T.A. Busbee, J.W. Boley, J.R. Raney, A. Chortos, A. Kotikian, J.D. Berrigan, M.F. Durstock, J.A. Lewis, Hybrid 3D printing of Soft electronics, Adv. Mater. 29 (40) (2017).
[14] Y. Tong, J.M. Murbach, V. Subramanian, S. Chhatre, F. Delgado, D.C. Martin, K.J. Otto, M. Romero-Ortega, B.N. Johnson, A hybrid 3D printing and robotic-assisted embedding approach for design and fabrication of nerve cuffs with integrated locking mechanisms, MRS Adv. 3 (40) (2018) 2365–2372.
[15] S. Yoon, J.A. Park, H.R. Lee, W.H. Yoon, D.S. Hwang, S. Jung, Inkjet-spray hybrid printing for 3D freeform fabrication of multilayered hydrogel structures, Adv. Healthc. Mater. 7 (14) (2018) e1800050.
[16] I. Raza, L. Iannucci, P.T. Curtis, Introducing a multimaterial printer for the deposition of low melting point alloys, elastomer, and ultraviolet curable resin, 3D Print. Addit. Manuf. 4 (2) (2017) 83–89.
[17] D. Espalin, J. Alberto Ramirez, F. Medina, R. Wicker, Multi-material, multi-technology FDM: exploring build process variations, Rapid Prototyping J. 20 (3) (2014) 236–244.
[18] R.B. Wicker, E.W. MacDonald, Multi-material, multi-technology stereolithography, Virtual Phys. Prototy. 7 (3) (2012) 181–194.
[19] A. Joe Lopes, E. MacDonald, R.B. Wicker, Integrating stereolithography and direct print technologies for 3D structural electronics fabrication, Rapid Prototyping J. 18 (2) (2012) 129–143.
[20] S.C. Ligon, R. Liska, J. Stampfl, M. Gurr, R. Mülhaupt, Polymers for 3D printing and customized additive manufacturing, Chem. Rev. 117 (15) (2017) 10212–10290.
[21] J. Jiang, X. Xu, J. Stringer, Support structures for additive manufacturing: a review, J. Manuf. Mater. Process. 2 (4) (2018) 64.
[22] Y. Jin, W. Chai, Y. Huang, Fabrication of stand-alone cell-laden collagen vascular network scaffolds using fugitive pattern-based printing-then-Casting approach, ACS Appl. Mater. Interfaces 10 (34) (2018) 28361–28371.
[23] Y. Jin, A. Compaan, W. Chai, Y. Huang, Functional nanoclay suspension for printing-then-Solidification of liquid materials, ACS Appl. Mater. Interfaces 9 (23) (2017) 20057–20066.
[24] H. Ding, R. Chang, Printability study of bioprinted tubular structures using liquid hydrogel precursors in a support bath, Appl. Sci. 8 (3) (2018) 403.
[25] T.J. Hinton, Q. Jallerat, R.N. Palchesko, J.H. Park, M.S. Grodzicki, H.-J. Shue, M.H. Ramadan, A.R. Hudson, A.W. Feinberg, Three-dimensional printing of complex biological structures by freeform reversible embedding of suspended hydrogels, Sci. Adv. 1 (9) (2015) 1–10.
[26] K. Kumar, G.S. Kumar, An experimental and theoretical investigation of surface roughness of poly-jet printed parts: this paper explains how local surface orientation affects surface roughness in a poly-jet process, Virtual Phys. Prototyp. 10 (1) (2015) 23–34.
[27] W.R.J. Priedeman, A.L. Brosch, Soluble Material and Process for Three-dimensional Modeling, Stratasys Inc., United State, 2004.
[28] R.J. Moon, A. Martini, J. Nairn, J. Simonsen, J. Youngblood, Cellulose nanomaterials review: structure, properties and nanocomposites, Chem. Soc. Rev. 40 (7) (2011) 3941–3994.
[29] R.J. Moon, G.T. Schueneman, J. Simonsen, Overview of cellulose nanomaterials, their capabilities and applications, JomUs 68 (9) (2016) 2383–2394.
[30] B.L. Peng, N. Dhar, H.L. Liu, K.C. Tam, Chemistry and applications of nanocrystalline cellulose and its derivatives: a nanotechnology perspective, Can. J. Chem. Eng. 89 (5) (2011) 1191–1206.
[31] Y. Habibi, L.A. Lucia, O.J. Rojas, Cellulose nanocrystals-chemistry, self assembly, and applications, Chem. Rev. 110 (2010) 22.
[32] T. Li, J. Aspler, A. Kingsland, L.M. Cormier, X. Zou, 3D printing – a review of technologies, markets, and opportunities for the forest industry, J. Sci. Technol. Forest Prod. Process. 5 (2) (2016) 30–37.
[33] W. Xu, X. Wang, N. Sandler, S. Willfor, C. Xu, Three-dimensional printing of wood-derived biopolymers: a review focused on biomedical applications, ACS Sustain. Chem. Eng. 6 (5) (2018) 5663–5680.
[34] W. Xu, A. Pranovich, P. Uppstu, X. Wang, D. Kronlund, J. Hemming, H. Oblom, N. Moritz, M. Preis, N. Sandler, S. Willfor, C. Xu, Novel biorenewable composite of wood polysaccharide and polylactic acid for three dimensional printing, Carbohydr. Polym. 187 (2018) 51–58.
[35] V.C.-F. Li, C.K. Dunn, Z. Zhang, Y. Deng, H.J. Qi, Direct ink write (DIW) 3D printed cellulose nanocrystal aerogel structures, Sci. Rep.-Uk 7 (1) (2017) 8018.
[36] V.C.F. Li, A. Mulyadi, C.K. Dunn, Y. Deng, H.J. Qi, Direct ink write 3D printed cellulose nanofiber aerogel structures with highly deformable, shape recoverable, and functionalizable properties, ACS Sustain. Chem. Eng. 6 (2) (2018) 2011–2022.
[37] X. Kuang, K. Chen, C.K. Dunn, J. Wu, V.C.F. Li, H.J. Qi, 3D printing of highly stretchable, shape-memory, and self-healing elastomer toward novel 4D printing, ACS Appl. Mater. Interfaces 10 (8) (2018) 7381–7388.
[38] M.K. Hausmann, P.A. Rühs, G. Siqueira, Jr. Läuger, R. Libanori, T. Zimmermann, A.R. Studart, Dynamics of cellulose nanocrystal alignment during 3D printing, ACS Nano 12 (7) (2018) 6926–6937.
[39] G. Siqueira, D. Kokkinis, R. Libanori, M.K. Hausmann, A.S. Gladman, A. Neels, P. Tingaut, T. Zimmermann, J.A. Lewis, A.R. Studart, Cellulose nanocrystal inks for 3D printing of textured cellular architectures, Adv. Funct. Mater. 27 (12) (2017) 1604619-n/a.
[40] M.A. Mohamed, W.S. WN, J. Jaafar, A.F. Ismail, M. Abd Mutalib, A.B. Mohamad, M.Z. MF, N.A. Awang, Z.A. Mohd Hir, Physicochemical characterization of cellulose nanocrystal and nanoporous self-assembled CNC membrane derived from Ceiba pentandra, Carbohydr. Polym. 157 (2017) 1892–1902.
[41] L. Du, J. Wang, Y. Zhang, C. Qi, M.P. Wolcott, Z. Yu, Preparation and characterization of cellulose nanocrystals from the bio-ethanol residuals, Nanomaterials (Basel) 7 (3) (2017).
[42] M.R.K. Sofla, R.J. Brown, T. Tsuzuki, T.J. Rainey, A comparison of cellulose nanocrystals and cellulose nanofibres extracted from bagasse using acid and ball milling methods, Adv. Nat. Sci. Nanosci. Nanotechnol. 7 (3) (2016) 035004.
[43] A. Kumar, Y.S. Negi, V. Choudhary, N.K. Bhardwaj, Characterization of cellulose nanocrystals produced by acid-hydrolysis from sugarcane bagasse as agro-waste, J. Mater. Phys. Chem. 2 (1) (2014) 1–8.
[44] J. Li, Y. Wang, X. Wei, F. Wang, D. Han, Q. Wang, L. Kong, Homogeneous isolation of nanocelluloses by controlling the shearing force and pressure in microenvironment, Carbohydr. Polym. 113 (2014) 388–393.
[45] M. Nacos, P. Katapodis, C. Pappas, D. Daferera, P. Tarantilis, P. Christakopoulos, M. Polissiou, Kenaf xylan – a source of biologically active acidic oligosaccharides, Carbohydr. Polym. 66 (1) (2006) 126–134.
[46] Q. Luo, Y. Shen, P. Li, C. Wang, Z. Zhao, Synthesis and characterization of cross-linking waterborne fluorinated polyurethane-acrylate with core-shell structure, J. Appl. Polym. Sci. 131 (21) (2014).
[47] J.B. Park, Y.-J. Kim, S.-M. Kim, J.M. Yoo, Y. Kim, R. Gorbachev, I.I. Barbolina, S.J. Kim, S. Kang, M.-H. Yoon, S.-P. Cho, K.S. Novoselov, B.H. Hong, Non-destructive electron microscopy imaging and analysis of biological samples with graphene coating, 2d Mater. 3 (4) (2016) 045004.
[48] E.T. Filipov, T. Tachi, G.H. Paulino, Origami tubes assembled into stiff, yet reconfigurable structures and metamaterials, Proc. Natl. Acad. Sci. U. S. A. 112 (40) (2015) 12321–12326.
[49] E.T. Filipov, G.H. Paulino, T. Tachi, Origami tubes with reconfigurable polygonal cross-sections, Proc. Math. Phys. Eng. Sci. 472 (2185) (2016) 20150607.
[50] Z. Zhao, X. Kuang, J. Wu, Q. Zhang, G.H. Paulino, H.J. Qi, D. Fang, 3D printing of complex origami assemblages for reconfigurable structures, Soft Matter 14 (39) (2018) 8051–8059.
[51] K. Liu, G.H. Paulino, Nonlinear mechanics of non-rigid origami: an efficient computational approach, Proc. Math. Phys. Eng. Sci. 473 (2206) (2017) 20170348.
[52] K.C. Cheung, T. Tachi, S. Calisch, K. Miura, Origami interleaved tube cellular materials, Smart Mater. Struct. 23 (9) (2014) 094012.
[53] D.K. Patel, A.H. Sakhaei, M. Layani, B. Zhang, Q. Ge, S. Magdassi, Highly stretchable and UV curable elastomers for digital light processing based 3D printing, Adv. Mater. 29 (15) (2017).